Investigation of Gadolinia-Doped Ceria (GDC) Electrolyte by Electrochemical Impedance Spectroscopy

ECS Transactions, 50 (27) 23-33 (2013)
10.1149/05027.0023ecst ©The Electrochemical Society

Investigation of Gadolinia-Doped Ceria (GDC) Electrolyte by Electrochemical Impedance Spectroscopy

Lei Zhang[a], Feng Liu[a], Kyle Brinkman[b], Anil V. Virkar[a]

[a] Department of Materials Science and Engineering, University of Utah, Salt Lake City, UT 84112, USA
[b] Savannah River National Laboratory, Aiken, SC 29808, USA

Electrochemical impedance spectroscopy (EIS) is widely used in the study of aqueous and solid state electrochemistry. Information such as sample conductivity and electrode effects can be studied by varying the frequency. Despite extensive use of EIS, two issues regarding the measurement and interpretation warrant discussion. They concern the high frequency inductive load and the use of constant phase element (CPE) for data fitting. The experimental work was conducted on polycrystalline gadolinia-doped ceria. In this work, subtracting lead impedance is shown to be an effective way to recover semi-circular behavior at high frequency, representative of grain boundary effects. The present work shows that in many instances for data interpretation, pure capacitance may be used in the equivalent circuit, instead of the often used CPE. The significance is that fitting can be achieved using one parameter rather than two needed for CPE.

Introduction

Electrochemical Impedance Spectroscopy (EIS) is a technique which measures the response of a sample under an AC stimulus in which the frequency is varied over a wide range. EIS has very wide applicability, and has been used for the study of ionic conductors, dielectric materials, semiconductors, solar cells, fuel cells, batteries and corrosion.

With the improvement in equipment over the years, four types of techniques have been used to measure the impedance. They are: AC bridge, Lissajous analysis, phase-sensitive detection and Fourier analysis. The most widely used technique involves the use of a single frequency input (at a time) followed by Fourier analysis. The general approach involves the application of a single frequency input and the measurement of the corresponding current (I) flow through and potential drop (V) across the sample. From the measurement of I and V, as well as the phase difference, the real and the imaginary parts of the impedance can be determined over a range of frequencies. In 1969, Bauerle investigated transport through yttria-stabilized zirconia (YSZ) samples with various applied electrodes and in several atmospheres using electrochemical admittance

spectroscopy, which is truly a landmark paper in the study of solid state ionics (1). Bauerle showed that the data could be fitted to semi-circles in the admittance plane. These semi-circles at high frequencies correspond to grain interiors and grain boundaries (1). He adopted pure resistance and pure capacitance to describe the equivalent circuit at high frequencies which accurately reproduced the measured spectra. Ever since, the use of EIS has become commonplace (2).

The resolution of grain and grain-boundary effects usually requires a high frequency input, often exceeding 100 kHz. It is well known that at high frequencies, there can be a significant contribution from an inductive load, the origin of which lies in the lead wires used to connect to the sample and other parts of the instrumentation. The effect of inductive load reflects as an imaginary part of the impedance below the x-axis when the real part is plotted on the x-axis and negative of the imaginary part is plotted on the positive y-axis. Thus, the capacitive effects appear above the x-axis and inductive effects below the x-axis. Many studies have shown that it is essential to subtract the effects of the leads before data can be adequately interpreted (2-4). In many recent studies, however, the approach used has been to ignore the part of the impedance that lies below the x-axis and fit the remaining portion above the x-axis (which is generally not semi-circular) using a CPE (5-9). The use of a CPE generally leads to a better fit to the data than using a capacitor. This of course is not surprising as fitting with a CPE requires two parameters unlike a capacitor, which requires only one parameter (8,9). However, the use of a CPE often makes it difficult to offer a unique physical interpretation as the fitting itself may lack uniqueness. In this work, we investigate GDC samples with the objective being the determination of grain and grain boundary ion transport properties. While many studies in the past have emphasized the need to remove the inductive contribution (2-4), the continual use of procedures in which the inductive part is cutoff suggests revisiting this issue would be fruitful.

Experimental Approach

Gd_2O_3-doped Ceria (GDC) powders were die-pressed into pellets and sintered in air at 1400°C. Pt paste was applied on both sides of the pellets and the pellets were fired at 800°C. The thickness of the pellet was 1.4 mm. Samples with two different electrode geometries (sizes) were used in this study; one set of samples with electrodes 15.8 mm in diameter and the other with electrodes 4.8 mm in diameter. Inset in Fig. 1 shows schematics of the two types of samples used.

Impedance spectra were obtained on the samples in air over a range of temperatures between 400^{o}C and 675^{o}C in 25 degree intervals. All impedance measurements were conducted using Solartron 1260 Frequency Response Analyzer. Impedance spectra over the same range were also obtained without the sample by connecting the two lead wires to each other. This gave inductive-resistive contribution of the lead wires and the testing setup. Fig. 1 shows an example of how the impedance was measured and interpreted. The corresponding equivalent circuits are shown as insets. The measured impedance of the whole setup including the sample is shown in Fig. 1a. Fig. 1b shows an enlarged part of the high frequency region of Fig. 1a. Impedance of the setup

without the sample with the leads shorted is given in Fig. 1c. The lead impedance (Fig. 1c) was then subtracted from the measured sample impedance (Fig. 1a). The difference, which should be the sample impedance, without the effects of the leads, is plotted in Fig. 1d. Finally, high frequency portion of the impedance from Fig. 1d is plotted in Fig. 1e. The data points in Fig. 1e are then fitted using a semicircle. As seen in Fig. 1e, the data can be fitted very well with a semicircle, which is representative of transport across grain boundaries. Also important to note is that the data point corresponding to the highest angular frequency (10^6 Hz) appears above the x-axis suggesting that the lead inductive-resistive effects have been removed.

Results and Discussion

Impedance data obtained over a temperature range from 400°C to 675°C before subtracting the lead impedance are plotted in Fig. 2a and Fig. 2b. The low frequency regime, as is well known, represents the electrode effects. In this paper only the high frequency effects were investigated. At low temperature (below 525°C) the effects of the lead impedance are not apparent (although still present) as the entire measured data over the range of frequencies lie above the x-axis. The near semicircular feature of the high frequency data can be seen in Fig. 2a. For temperatures 550°C and above (Fig. 2b), the high frequency regime appears as a depressed semicircle. At the measurement temperatures of 650°C and 675°C, the high frequency arc is not even observed. Also, lead inductive effects are clearly seen at higher temperatures, as evidenced by part of the measured impedance data lying below the x-axis. The lead impedance comprising inductive and resistive contributions was found to be nearly independent of temperature, unlike the sample impedance which rapidly decreases with increasing temperature. As such, the effects of the leads relative to the sample become more significant at higher temperatures.

Fig. 2c and Fig. 2d show the same data, respectively from Fig. 2a and Fig. 2b, but from which the lead impedance have been subtracted. Thus, data in Fig. 2c and Fig. 2d represent the sample impedance without any lead effects. All high frequency arcs now appear perfectly semicircular. Also, no data points lie below the x-axis clearly showing that the effects of the leads have been subtracted out. Also note that even at the highest measurement temperature of 675°C, the high frequency semicircular arc is clearly visible. Fig. 2e and Fig. 2f respectively show the measured data at 650°C and 675°C, in which the plots include measurements with and without lead effects. As clearly seen, the semicircle representing grain resistance, grain boundary resistance, and grain boundary capacitance can be clearly resolved once the lead impedance is subtracted, unlike the raw measured data in which no high frequency arcs can be seen.

In all cases, the semicircles were extrapolated to the x-axis. The high frequency intercept of the semicircle corresponds to the area specific grain resistance, R_g, and the low frequency intercept

corresponds to the area specific grain + grain boundary resistance, namely, R_g+R_{gb} (1). The corresponding Arrhenius plots, namely, $\ln(\frac{R_g}{T})$ vs. $\frac{1000}{T}$ and $\ln(\frac{R_{gb}}{T})$ vs. $\frac{1000}{T}$ are shown in Fig. 3. In Fig. 3a and Fig. 3b raw data are shown on Arrhenius plots. The data exhibit linear behavior on Arrhenius plots up to a temperature of ~500^{o}C. Above this temperature, the high frequency arc is not resolved clearly in the impedance spectra. This reflects as apparent deviation from the linear behavior on Arrhenius plots and the corresponding error is ~20 Ωcm^2. Fig. 3c and Fig. 3d show the same data by subtracting the lead impedance. The linear behavior on Arrhenius plots is now observed up to a temperature of 600^{o}C and the corresponding error level is reduced to ~2 Ωcm^2. The data shown in Fig. 3a through Fig. 3d were obtained on a sample with large platinum electrode area (15.8 mm diameter) and with platinum leads. Similar data were also obtained with large platinum electrodes but with silver leads. The reason for using silver was to further reduce the lead resistance. These data after subtracting the lead impedance are shown in Fig. 3e and Fig. 3f. In this case also the linear behavior is observed up to ~600^{o}C. However, the error level was ~6 Ωcm^2 indicating little further improvement occurred by using silver leads. Finally, Fig. 3g and Fig. 3h show data obtained using small platinum electrodes (4.8 mm) and with silver leads, after subtracting out the lead impedance. The linear behavior is now observed up to ~675^{o}C and the error level is further reduced to ~1 Ωcm^2. The present results thus indicate that by a suitable choice of sample geometry and subtracting the lead impedance, the high frequency arc can be fitted well to a semicircle consistent with the description of the grain boundary effects using a resistor and a capacitor, as originally shown by Bauerle in his landmark paper (1). It should be further possible to choose samples with appropriate geometry and suitable leads to increase its resistance relative to the lead impedance and extend the linear regime of Arrhenius plots to even higher temperatures.

The data from Figs. 3a, 3c, 3e and 3g can be fitted to

$$R_g = R_g^o T \exp(-\frac{Q_g}{RT}) \quad (1)$$

for the grain resistance with R_g^o as the pre-exponent (units of Ωcm^{2}K^{-1}) and Q_g as the activation energy. Similarly, data from Fig. 3b, 3d, 3f and 3h can be fitted to

$$R_{gb} = R_{gb}^o T \exp(-\frac{Q_{gb}}{RT}) \quad (2)$$

for the grain boundary resistance with R_{gb}^o as the pre-exponent (units of Ωcm^{2}K^{-1}) and Q_{gb} as the activation energy. The corresponding activation energies are listed in Table 1. The data obtained with small electrodes and silver wires correspond to the largest linear range on the Arrhenius plots. The corresponding measured activation energies are $Q_g \cong 0.69$ eV and $Q_{gb} \cong 1.11$ eV. These values are typical of reported data on ceria (10).

From the high frequency semicircle, the grain boundary capacitance can be obtained from the maximum in –ImZ(ω). This is given by

$$C_{gb} = \frac{1}{\omega_m R_{gb}} \quad (3)$$

where ω_m is the angular frequency at which –ImZ(ω) is a maximum. Fig. 4a shows the raw impedance data obtained at 600°C on a sample in which some data points are below the x-axis. In Fig. 4b, the inductive effects (below the x-axis) are cutoff and the high frequency portion is fitted with a CPE, a procedure used in some of the reported studies. It is clear that the arc cannot be fitted with semi-circle. Fig. 4c shows the same data as in Fig. 4a but after subtracting the lead impedance. The high frequency portion of the arc is fitted using a semicircle in Fig. 4d. As clearly seen in Fig. 4d, the data can very accurately fitted using a capacitor and does not require a CPE. The obtained fit with a CPE in Fig. 4b, in which part of the impedance below the x-axis was simply cutoff does not correspond to the sample impedance only, but also includes the effects of the leads. Thus, the corresponding parameters of the CPE cannot be uniquely assigned to the sample. In addition, note that arc intercept on the x-axis with CPE fitting by cutting off impedance below the x-axis (Fig. 4b) extends between ~17 Ωcm^2 and ~27 Ωcm^2. However, when the lead impedance is subtracted out, the intercept of the semicircle on the x-axis (Fig. 4d) extends between ~3.7 Ωcm^2 and ~20.5 Ωcm^2. These intercepts in Fig. 4d can be identified respectively with R_g and $R_g + R_{gb}$, unlike the intercepts in Fig. 4b.

The area specific C_{gb} determined using data obtained with Pt and Ag leads with large Pt electrodes and Ag leads with small Pt electrodes are plotted in Fig. 5 vs. the measurement temperature. Data obtained with large electrodes show an increase with increasing temperature above about 600°C. This, however, is an artifact of measurement in which significant errors occur in resolving the spectra for the aforementioned reasons. The data obtained with small electrodes, however, show that the measured grain boundary capacitance is essentially independent of temperature over the range of temperatures data were obtained. This is consistent with expectations in that the grain boundary capacitance is likely determined by grain boundary structure and chemistry (11-14), which is virtually frozen in at low temperatures over which measurements were made.

Summary

In this work, EIS measurements were made on GDC disc-shaped samples with Pt electrodes of two different sizes; 4.8 mm in diameter and 15.8 mm diameter. Measurements were made over a range of temperatures between 400°C and 675°C in 25 degree intervals. The lead/instrument impedance was separately measured by shorting the lead wires without the sample. Above ~500°C, the high frequency spectra of the samples appeared to be flattened semicircles. At 650°C and 675°C, no high frequency arcs were observed. Also, significant portion of the measured

impedance at frequencies was below the x-axis consistent with contribution from the lead inductance. When the lead impedance was subtracted from the measured total (sample + lead) impedance, high frequency semicircular arcs could be recovered at the highest measurement temperature of 675°C. Also, the arcs could be fitted accurately with a semicircle in each case, consistent with the corresponding equivalent circuit being a resistor and a capacitor in parallel. From the measurements, after subtracting the lead impedance, the grain resistance, R_g, the grain boundary resistance, R_{gb}, and the grain boundary capacitance, C_{gb}, could be resolved. The grain resistance and the grain boundary resistance exhibited thermally activated behavior with the corresponding activation energies of $Q_g \cong 0.69$ eV and $Q_{gb} \cong 1.11$ eV, respectively. The grain boundary capacitance was essentially independent of temperature. The present work highlights the importance of subtracting the lead impedance (2-4). Once the lead impedance is subtracted out, the high frequency arc could be accurately fitted with a capacitor (one parameter) and it was not necessary to use a CPE (which requires two fitting parameters).

Acknowledgement

This work was supported by the US Department of Energy under its Energy Frontier Research Centers (EFRC) program under Grant Number DE-SC0001061 as a flow-through from the University of South Carolina, HeteroFoam Center. Part of this work was also supported by Savannah River National Lab under subcontract number AC72315-O.

References

1. J.E. Bauerle, *J. Phys. Chem. Solids* **30**, 2657 (1969).
2. E. Barsoukov, J. R. Macdonald, *Impedance Spectroscopy: Theory, Experiment, and Applications*, Wiley-Interscience (2005).
3. A. Esquirol, N. P. Brandon, J. A. Kilner, M. Mogensen, *J. Electrochem. Soc*., **151** (11) A1847-A1855 (2004).
4. A. Samson, M. Sogaard, R. Knibbe, N. Bonanos, *J. Electrochem. Soc*., **158** (6) B650-B659 (2011).
5. T. Suzuki, B. Liang, T. Yamaguchi, H. Sumi, K. Hamamoto, Y. Fujishiro, *J. Power Sources* **199**, 170 (2012).
6. A. Torabi, A. R. Hanifi, T. H. Etsell, P. Sarkar, *J. Electrochem. Soc.* **159** (2), B201 (2012).
7. J. Wang, Y. Zhang, T. Liang, C. Deng, J. Xu, *J. Power Sources* **208**, 415 (2012).
8. W. Zając, J. Molenda, *Solid State Ion.* **192**, 163 (2011).
9. W. Zając, J. Molenda, *Solid State Ion.* **179**, 154 (2008).
10. B.C.H. Steele, *Solid State Ion.* **129**, 95 (2000).
11. K. Lehovec, *J. Chem. Phys*., **21** (7) 1123-1128 (1953).
12. K. L. Kliewer and J. S. Koehler, *Phys. Rev.*, **140** (4A) A 1226-A1240 (1965).
13. X. Guo and J. Maier, *J. Electrochem. Soc*., **148** (3) E121-E126 (2001).
14. X. Guo, W. Sigle and J. Maier, *J. Am. Ceram. Soc*., **86** [1] 77-87 (2003).

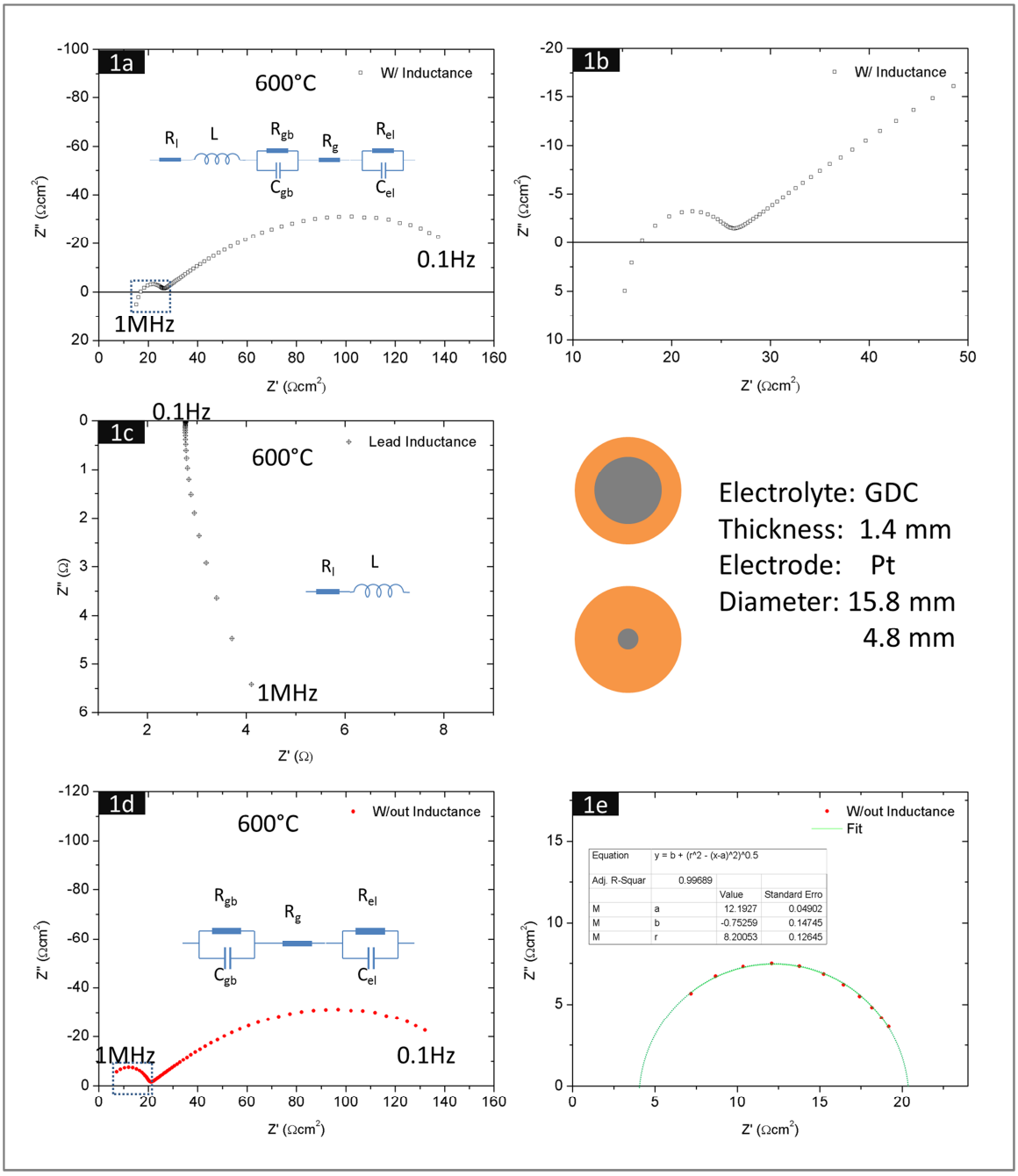

Figure 1: Experimental approach used for impedance measurement and data interpretation. a) Measured impedance of the whole setup, including the sample and the lead impedance; b) Enlarged view of the high frequency region in a; c) Measured lead impedance by shorting the leads without a sample; d) Sample impedance obtained by subtracting the lead impedance (c) from the measured sample-setup impedance (a); e) Enlarged view of the dashed part in (d). These data are fitted to a semicircle. From the semicircle, the grain resistance, the grain boundary resistance and the grain boundary capacitance are readily obtained.

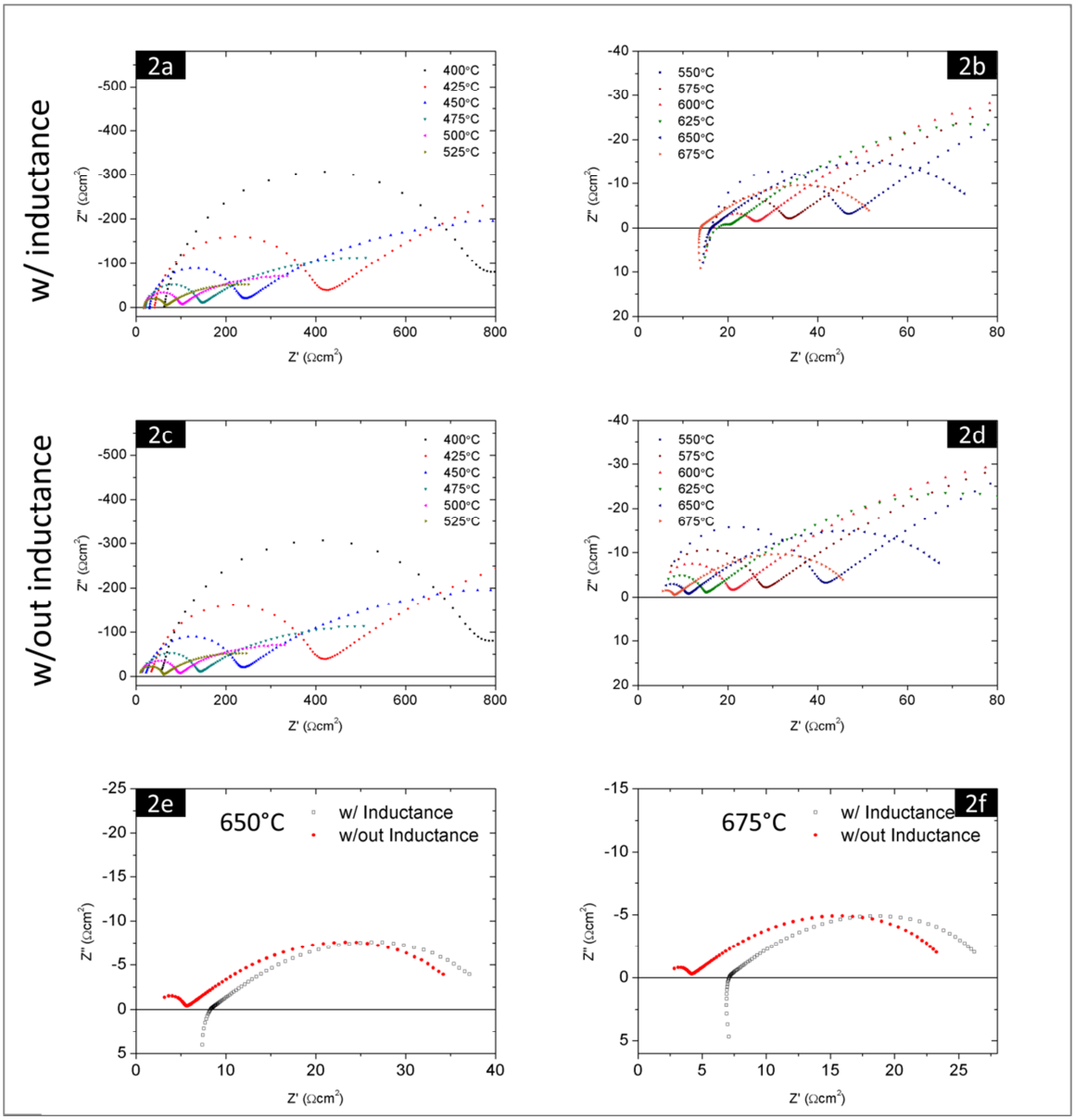

Figure 2: a) and b) are the as-measured impedance plots for the sample including the setup from 400°C to 675°C; c) and d) are the corresponding impedance plots after subtracting the lead impedance over the same temperature range; e) and f) compare the plots with and without the leads effects at 650°C and 675°C, respectively. Note that once the lead effects are subtracted out, the high frequency arcs appear and that they are semi-circular in shape.

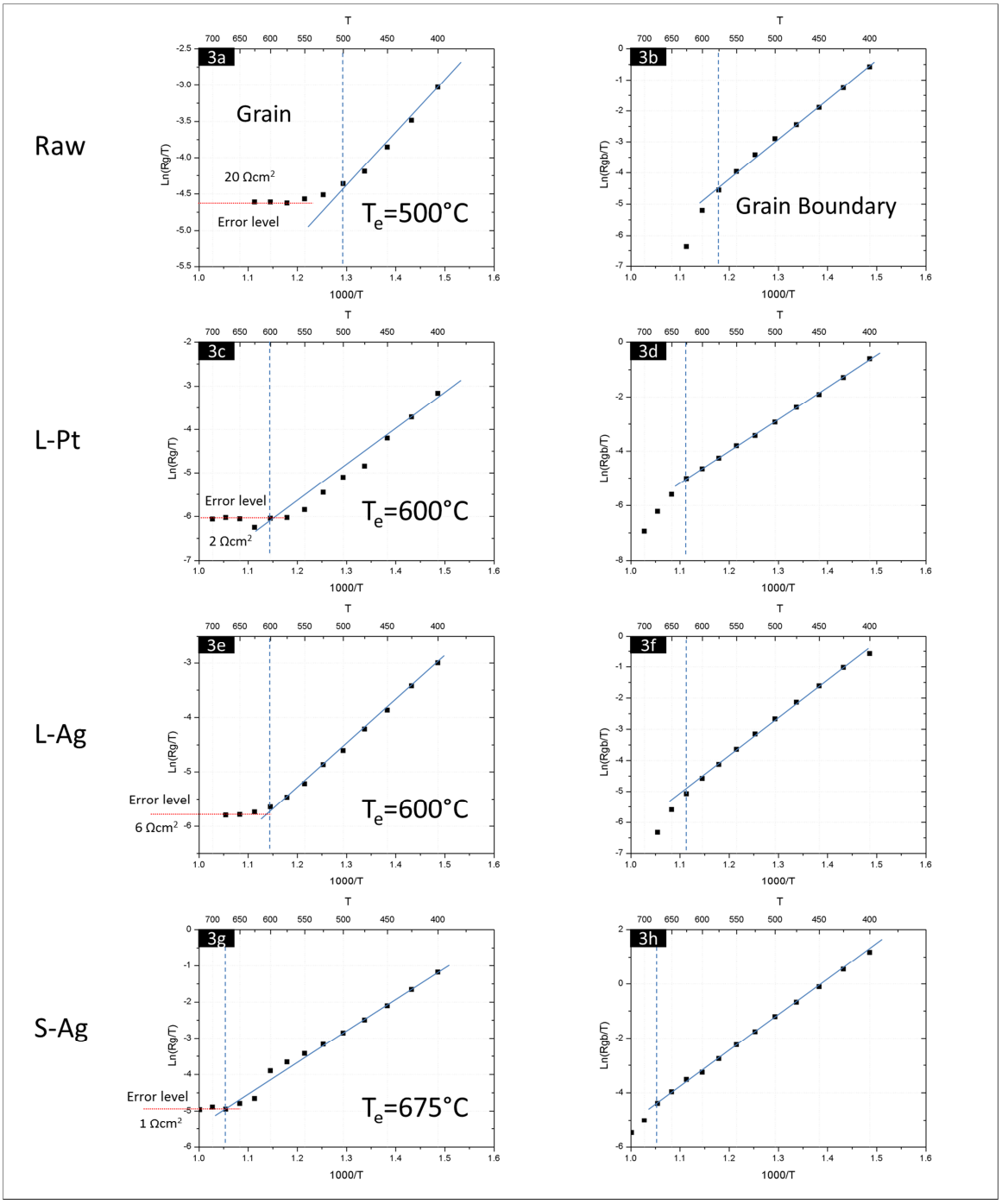

Figure 3: Arrhenius plots corresponding to ln $\left(\frac{R_g}{T}\right)$ vs.$\frac{1000}{T}$ (a, c, e, g) and ln($\frac{R_{gb}}{T}$) vs. $\frac{1000}{T}$(b, d, f, h) where $R_g$is the grain resistance and $R_{gb}$is the grain boundary resistance. (a) and (b) correspond to intercepts obtained on large Pt electrode and Pt leads without subtracting the lead impedance. (c) and (d) correspond to intercepts obtained using data from (a) and (b) but after subtracting the lead impedance. (e) and (f) correspond to intercepts obtained with large Pt electrodes and silver leads after subtracting the lead impedance. (g) and (h) correspond to intercepts obtained with small Pt electrodes and Ag leads after subtracting the lead impedance.

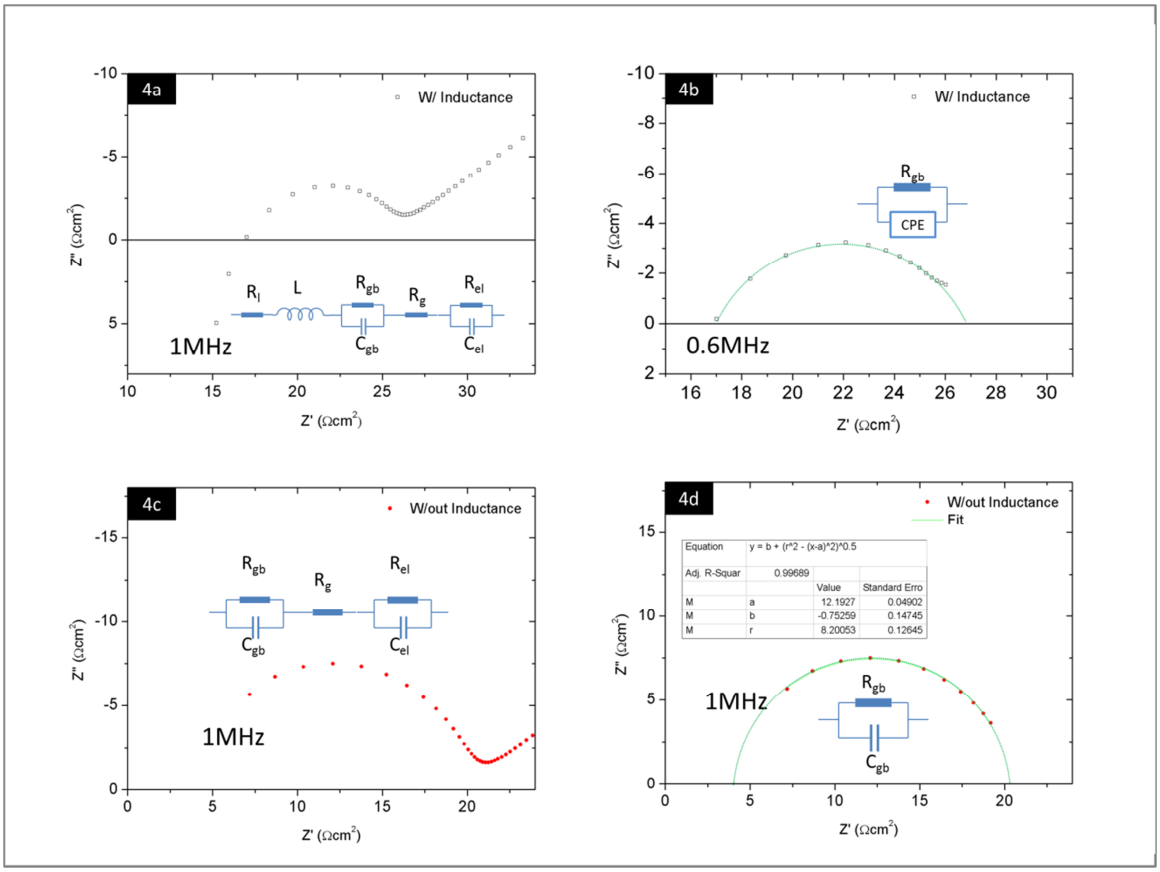

Figure 4: Comparison between inductance subtraction and inductive cut-off, as well as between capacitance-fitting and CPE-fitting. a) The high frequency regime of the measured impedance with large Pt electrodes at 600°C. b) The high frequency arc from (a) after cutting off data below the x-axis. The arc is not semicircular and was fitted as a CPE. c) The high frequency arc from (a) after subtracting the lead impedance. d) The high frequency arc from (c). The arc could be accurately fitted as a semicircle.

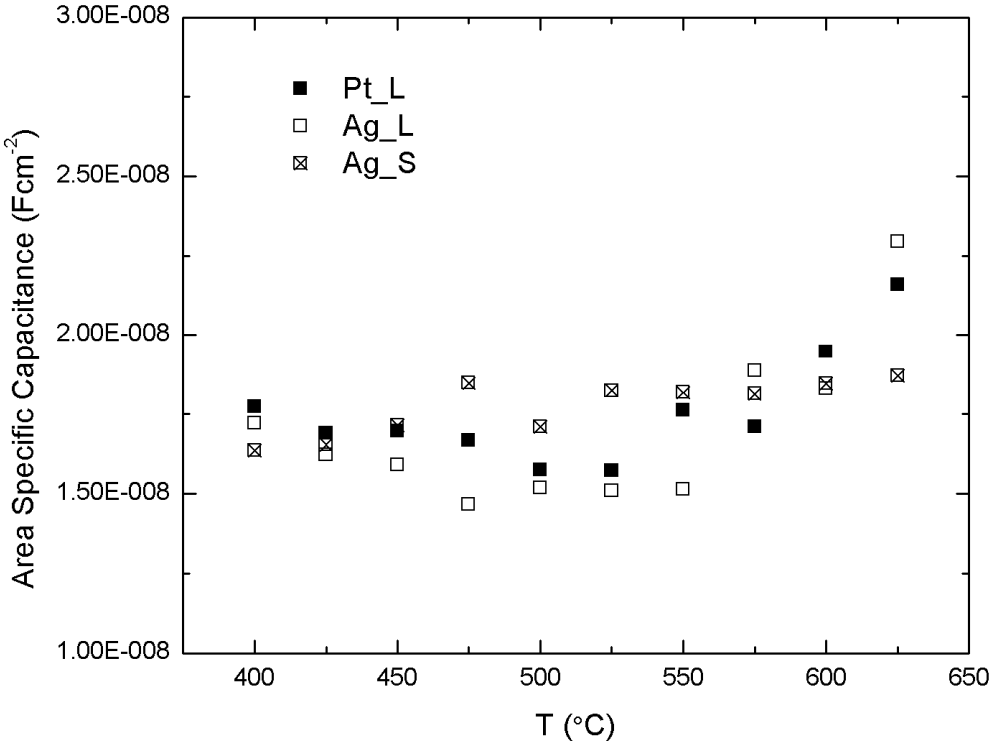

Figure 5: Area Specific Grain Boundary Capacitance, C_{gb}, obtained by fitting to the high frequency semicircle. Pt_L corresponds to the sample with large electrodes and measured using Pt leads; Ag_L corresponds to the sample with large Pt electrodes and measured using Ag leads; Ag_S corresponds to the sample with small Pt electrodes and measured using Ag leads.

Table-1 Activation energies

	Q_g (eV)	Q_{gb} (eV)
Raw	0.67	1.05
L-Pt	0.73	1.01
L-Ag	0.7	1.03
S-Ag	0.69	1.11
Literature	0.78	